CONTROL OF RADIOACTIVE WASTE-GLASS MELTERS: Part 2 - Residence Time and Melt Rate Limitations (U)

Dennis F. Bickford[1], Pavel Hrma[2] and Bradley W. Bowan II [3]

[1]*Westinghouse Savannah River Co., Savannah River Laboratory, Aiken, SC 29802.*
[2] *Case Western Reserve University, Cleveland, OH 44106.*
currently with Battelle Pacific Northwest Laboratories, Richland, WA 99352.
[3] *West Valley Nuclear Services Co., P.O. Box 191, West Valley, NY 14171.*

American Ceramic Society Manuscript 199442P

for publication in the Journal of the American Ceramic Society

CONTROL OF RADIOACTIVE WASTE-GLASS MELTERS: Part 2 - Residence Time and Melt Rate Limitations

Dennis F. Bickford[1], Pavel Hrma[2] and Bradley W. Bowan II [3]

[1]*Westinghouse Savannah River Co., Savannah River Laboratory, Aiken, SC 29802.*
[2] *Case Western Reserve University, Cleveland, OH 44106.*
currently with Battelle Pacific Northwest Laboratories, Richland, WA 99352.
[3] *West Valley Nuclear Services Co., P.O. Box 191, West Valley, NY 14171.*

ABSTRACT

Slurries of simulated high level radioactive waste and glass formers have been isothermally reacted and analyzed to identify the sequence of the major chemical reactions in waste vitrification, their effect on glass production rate, and the development of leach resistance.

Melting rates of waste batches have been increased by the addition of reducing agents (formic acid, sucrose) and nitrates. The rate increases are attributable in part to exothermic reactions which occur at critical stages in the vitrification process. Nitrates must be balanced by adequate reducing agents to avoid the formation of persistant foam, which would destabilize the melting process. The effect of foaming on waste glass production rates is analyzed, and melt rate limitations defined for waste-glass melters, based upon measurable thermophysical properties.

Minimum melter residence times required to homogenize glass and assure glass quality are much smaller than those used in current practice. Thus, melter size can be reduced without adversely affecting glass quality.

Physical chemistry and localized heat transfer of the waste-glass melting process are examined, to refine the available models for predicting and assuring glass production rate. It is concluded that the size of replacement melters and future waste processing facilities can be significantly decreased if minimum heat transfer requirements for effective melting are met by mechanical agitation.

A new class of waste glass melters has been designed, and proor of concept tests completed on simulated High Level Radioactive Waste slurry. Melt rates have exceeded 155 kg m^{-2} h^{-1} with slurry feeds (32 lb ft^{-2} h^{-1}), and 229 kg kg m^{-2} h^{-1} with dry feed (47 lb ft^{-2} h^{-1}) . This is about 8 times the melt rate possible in conventional waste-glass melters of the same size.

INTRODUCTION

High Level Radioactive Waste (HLW) is the residue of chemical reprocessing of uranium fuel and targets after irradiation in nuclear reactors. HLW contains most of the fission products of irradiation, including the intense beta and gamma radiation emitters Cs^{137} and Sr^{90}. The presence of these fission products requires that processes to store and dispose of HLW guard against both physical transfer to the environment (contamination) and energy transfer (irradiation). As a result, HLW storage and processing facilities are designed for remote maintenance and repair, and typically include the equivalent of 1.5 meters or more of reinforced concrete shielding.

In the United States most of the HLW is stored at Department of Energy facilities. The Hanford reservation, in Richland, Wash., has over 2.3×10^8 liters (60 million gallons), the Savannah River Site has over 1.1×10^8 liters (30 million gallons). At both of these sites the majority of the waste has been pH adjusted with sodium hydroxide, and is stored in underground carbon steel tanks. The remainder of defense related HLW is stored as 1.1×10^7 liters (3 million gallons) of dry calcine at the Idaho Chemical Processing Plant, Idaho Falls. From 1966 to 1971 Nuclear Fuel Services Co. reprocessed spent fuel rods from commercial power reactors to make more fuel. As a result of those operations about 2.3×10^6 liters (0.61 million gallons) of commercial HLW are now stored at the West Valley Demonstration Project (WVDP),West Valley, New York.

Nuclear waste-glass for permanent disposal is prepared by melting a slurried mixture of solid nuclear waste (which may be partly dissolved in water) and glass frit or glass forming chemicals [1-6]. Laboratory and pilot scale operations have been conducted in the US, Europe and Japan to develop equipment, borosilicate glass compositions, and process control methods. Unlike commercial glass melters, which are built where they are operated, HLW glass melters are constructed as integrated systems and moved to the operating facilities. At the facilities they are installed and removed using remotely operated cranes. Once installed the maintenance of these melters is limited to changing out of auxiliary devices, and complete melter replacement. This operating environment requires melters of limited size that produce glass of consistant quality at predictable rates.

Figure 1 illustrates the types of melter systems that have been developed. The melters fall into three general classes; batch melters, continuous pot melters, and Joule-heated ceramic-lined melters.

The first waste glass melters were designed for batch operations, a direct increase in scale from glass development crucible tests. This approach was found unsuitable for production facilities because of low melt rates caused by slow heat transfer from external heaters through the canister into the reacting batch. Lack of agitation and temperature nonuniformities also made it difficult to homogenize the glass. Calcination of feed before introduction into the canister increased the melt rate but also increased the tendency for crystal formation in the glass, and entrained part of the waste in the calciner offgas system. This method was finally eliminated based on the large number of melters, operating in parallel, necessary to meet the production rates required to dispose of HLW inventories.

The second class of melters developed were continuous pot melters. In this type the melt rate was improved by increasing the diameter of the pot, by direct heating of the pot by radio frequency induction heating, and by continuous feeding of raw materials. Glass homogeneity was improved by using gas bubblers to agitate the melt. The largest of this type of melter is the French AVH system which melts 25 kg per hour (55 pounds per hour). This is the processing rate limit per pot melter using dried feed: With slurry feeding the melter capacity limit is about one half of this. The melter size and temperature is limited to below 1050°C by creep resistance of the nickel-chromium alloy used for the pot.

The third category of melters are the joule-heated ceramic-lined melters. In this class the melter is lined with refractory, and the glass is joule heated by electricity transferred through the melt between nickel-chromium alloy electrodes. An example of a joule-heated ceramic-lined production melter is shown in Figure 2. This class of melters with slurry feeding has been selected for all the production melter systems in the US, W. Germany and Japan because of the high production rate and high glass quality. The size of these systems is limited only by replacement crane capacity and facility space, since all the structural support is provided by a stainless steel shell which contains the refractory. The electrodes only need to be self supporting, and high current densities are possible on the faces of the electrodes [7], therefore nominal melt temperatures can be as high as 1150°C, which is only 200°C lower than the electrode melting point [7,8].

Glass production rates are approximately proportional to the surface area of the melt, but convection caused by the joule heating is enhanced as the size of the melter is increased, so larger melters have proportionately higher melt rates. Laboratory melters with melting areas smaller than 0.09 m^2 (1 ft^2) operate below 22 kg m^{-2} h^{-1} (4.5 lb ft^{-2} h^{-1}), pilot scale and production melters up to 2.15 m^2 (23.1 ft^2) operate at rates up to 39 kg m^{-2} h^{-1} (8 lb ft^{-2} h^{-1}). Increased melt rates have been demonstrated through 1) the addition of lid booster heating, 2) adjusting the proportion and composition of ground glass frit and batched chemicals, 3) increased use of reducing agents (e.g. formic acid, sucrose), 4) use of surface active species (e.g. sulfates, halides), and 5) through increased melter convection (lower glass viscosities, higher operating temperatures, power skewing to bottom electrodes, mechanical agitation by bubblers). During pilot scale experiments melt rates have also been doubled by dry feeding.

A variety of analytical, physical and finite element models have been developed to aid in optimizing and assuring that production waste-glass melters would be capable of reference melt rates [9-12]. For a given melter feed, glass melt rates can be modeled to within 10% of experimentally determined values using a heat transfer model with measured glass properties, and only one adjustable parameter, used to estimate the effectiveness of lid heaters [12]. Thus, melt rates can be reliably predicted for modest changes in melter size, and operating conditions. However, none of the available models have been successful in predicting the melt rate for significant changes in melter feed composition. In all the available models the reacting batch is modeled by constant or continuous functions based on the final glass product's composition, and therefore cannot account for the effects of actual reactions in the melt. In most cases the

models rely on an estimated or empirically determined heat transfer coefficient between the bulk glass and the reacting batch to account for glass feed characteristics, and therefore cannot predict glass melt rates a priori.

Since all the available models are based on similar melter geometries, where a water slurry is directly fed to the top of a molten glass pool, the models cannot be used to simulate alternative geometries. Addition of a mechanically driven agitator to a commercial electric glass furnace has been reported to raise the melt rate for dry feeding to 1221 kg m^{-2} h^{-1} (250 lb ft^{-2} h^{-1}) [20], as compared to conventional commercial glass melters which operate at the rate of 100 kg m^{-2} h^{-1} (20 lb ft^{-2} h^{-1}) . Concerns with slurry feeding of an agitated melter included stability of the melt with liquid water present, glass quality, melt rate, ability of the melter to defoam the batch, and melter materials compatibility. Results are reported of proof of concept tests for slurry feeding of an agitated melter of a new design.

The purpose of the following analysis is to determine what reactions are critical for the development of waste-glass durability, how foaming is related to gas evolution and melt viscosity, how batch reactions and foaming affect the melting rate, and what are the conditions for steady melting. Minimum melter residence time to develop glass durability is assessed. The sequence of melt reactions is determined, and related to heat requirements and the development of foam. Formulas relating the batch melting rate and foam layer thickness to foam porosity, batch melting rate and other variables will be developed. It will be suggested that more uniform performance will result if waste glass melters are operated at constant melting viscosity rather than constant melting temperature. Melt modeling will be used to estimate the minimum possible melter volume for a given production rate, and agitated melting will be discussed for a reduced-volume, high-melt-rate melter.

EXPERIMENTAL

Isothermal fusions of four simulated waste glass batches have been conducted to determine the kinetics of waste glass fusion, and the minimum melter residence time and temperature for minimal glass leachability. Slurry samples from melter tests SGM3, and SGM6 at SRL, and SF8 and SF9 at WVDP were used as typical melter feeds. Corresponding glass compostions are given in Table 1. The WVDP slurrys were prepared from batch chemicals, including colloidal silica; the SRL feeds used ground glass frit as the primary source of silicon, listed in Table 2. Samples were fused for 1/4, 1/2, 1, 2, and 4 hours at 650, 750, 850, 950, and 1150°C. The 30 ml slurry samples were contained in 100 ml high purity alumina crucibles, with fitted lids. Samples were supported by an alloy carrier, with 1.5 cm thick insulating firebrick covering the sides, and 5 cm thick insulating firebrick covering the top. The insulation caused the majority of the heat to enter through the bottom of the crucible, simulating the upward flow of heat in a slurry fed melter. The carriers were placed into preheated furnaces, removed after the specified times, and air cooled to room temperature. Cooled crucibles and samples were sectioned vertically with a high-speed water-cooled diamond saw.

The cross-sectioned, partially-reacted samples were visually examined for glass/foam structure, and gauged for foam height. Volumes of the foamed glasses were calculated relative to the volume of the final melts. Results for Savannah River "coupled" glasses, where the majority of alkali and boron are in aqueous solution, were comparable to melt volumes directly observed by Ahn for SRL "sludge only" melts, where the majority of alkali and boron were contained in the frit [13]. The structures were divided by appearance into 10 reaction stages, ranging from dried batch, to final glass with no visible porosity. See Table 3 for a description of the individual stages, and the corresponding average foam volume for each stage. Each sample was assigned a stage number, based upon this description. The resulting stage numbers are plotted in Figure 3, for the four melter feed types (SGM3, SGM6, SF8, SF9) versus isothermal reaction time (1/4, 1/2, 1, 2, 4 h) and temperature (650, 750, 850, 950, 1150°C).

Powder from each sample was mixed in the approximate ratio of 10:1 with silicon powder, and analyzed by X-ray powder diffraction to determine the rate and sequence of chemical reactions. The area of the largest characteristic X-ray peak, for each identified crystalline phase, was ratioed to the Si (111) peak area, multiplied by the actual mass ratio of sample to silicon standard. The silicon internal standard was used to correct for possible variations in sample preparation and X-ray absorbtion. In a few samples the major peaks coincided, and secondary peaks were used, and corrected using ideal peak area ratios. The results are given in Table 4, for baseline samples reacted for 4 hours at 400°C, and in Figure 4 for the test matrix samples.

Portions of the four slurry batchs were dried in air at 80 °C for 24 h, and analyzed by thermogravimetric analysis (TGA) and differential scanning calorimetry (DSC). DSC was calibrated using the heat of fusion of silver [15,16]. Similarly dried samples of formated sludge components, and formated sludge components mixed with sodium nitrate, were also analyzed by DSC. A summary of the results is given in Table 5.

The melter feed content of the major redox species in each of five feed batches is given in Table 6, together with experimentally determined melt rates on the SRL Scale Glass Melter (SGM), or the West Valley Slurry Fed Melter (SF). Maximum melt rates were the maximum that could be sustained over a 6 hour period. Direct visual examination and thermocouple probing of the reacting batch indicated that the reacting layer was 5 to 10 cm thick during continuous melting.

One half of each of the samples was ground with an agate mortar and pestle. A portion of the powder for each sample was analyzed for Fe(II)/Fe(III) using the colorimetric method of Reference 14. Results are plotted versus reaction time and temperature in Figure 4. A modified Corning Glass Works powder leach test method was used to measure durability: 1 gram samples of < 200 μm diameter powders were heated for 2 hours at 80°C in 100 ml of deionized water contained in sealed 250 ml polyethelene bottles. After cooling, each leachate was decanted. The pH of the decanted solution was determined, one drop of ultrex nitric acid added, and the leachates digested for 24 hours at 80°C. The leachates were then analysed by inductively coupled plasma emission spectroscopy (ICP). Leachate concentrations were plotted versus reaction time and temperature. This test method has been shown to correlate well with other

standardized leach test methods [17]. Figure 5 contains typical results for pH and the major soluble species sodium and boron. Silica X-ray data are included in Figure 5 as an indication of the rate of glass homogenization. Quartz was a minor component in batches SGM3 and SGM6, and the major source of SiO_2 in SF8 and SF9.

A 40 wt % slurry similar to that of SGM6 was melted in a mechanically agitated, Joule-heated melter of new design [18,19]. The agitated melter is related to an experimental glass melter developed to conduct the primary melting of commercial E-glass [20]. Stable melt rates exceeded 155 kg m^{-2} h^{-1} with slurry feeds (32 lb ft^{-2} h^{-1}), and 229 kg m^{-2} h^{-1} with dry feed (47 lb ft^{-2} h^{-1}) when the melter was operated at 1075 °C. Melt rate with the agitator not rotating was 19.5 kg m^{-2} h^{-1} (4.0 lb ft^{-2} h^{-1}). Glass samples were examined for durability and porosity. Initial operations produced glass with approximately 20% porosity. Through further design changes the porosity in the product was essentially eliminated, as determined by examination of fractured surfaces, and density measurements.

DISCUSSION

Development of Aqueous Leach Resistance, Minimum Melter Residence Time

As is shown in Figure 5, at the nominal operating temperature for the DWPF melter (1150°C) the crucible fusion of small samples occurs in about 15 minutes. Extending the melting to 4 hours improves durability only slightly. In fact, most of the homogenization and improvement in leach resistance occurs within the first hour, at temperatures as low as 850°C. This is supported by the X-ray diffraction data in Figure 5, which indicates essentially complete colloidal silica dissolution in molten waste-glass after only 1 hour at 850°C. Sample SGM3 did not have sufficient crystalline silica in its feed to yield a silica X-ray pattern, and is inferred to be similar to SGM6, since their leach performances are comparable. This behavior is supported by the results of devitrification studies, where the exsolution of up to 8 volume % spinel had negligable effect on glass durability [21,22]. Characteristic boron or aluminum compound X-ray patterns were not found in isothermal melting samples, implying that they rapidly join with the available alkali to form an early molten phase.

Comparison of the crystalline development of iron phases during melting, and devitrification (Ref. 11) leads to the conclusion that spinel crystal dissolution and exsolution is a thermodynamicly controlled property, since similar results can be achieved through opposite reaction paths. However, the formation of acmite ($NaFeSi_2O_6$) is common in devitrification, but was not seen in any of the isothermal melting tests, implying that acmite is a metastable phase resulting from limited iron and silica mobility during waste glass cooling.

The potential economic and melter design impact of the determination of the minimum required residence time is substantial. The reference DWPF melter design contains 6100 kg of glass, which results in an average residence time of 59 hours for the reference glass production rate of 104 kg h^{-1}. In alternative designs, if the average residence time

were reduced to 4 hours, less than 10% of the current glass inventory would be required to meet residence time requirements. For a given amount of insulation, the mass of a melter is proportional to its surface area, or (volume) $^{2/3}$. Thus, on a theoretical basis, waste-glass melters can be reduced to about 15% of their current mass, provided that minimum heat transfer rates can be met. Further consideration of this concept is discussed below.

Effect of Heat Capacity on Melt Rate

One possible means of modifying the existing heat transfer models to account for differences in batch melt rates is through improvement in the estimation of the enthalpy required to convert dried slurry to homogeneous glass. Most models assume melt rates to be a linear function of the inverse of the heat capacity, and use heat capacity of the final glass to estimate the heat capacity of the reacting batch.

Heat capacities, and other thermophysical properties have been measured by Pye and coworkers on simulated radioactive waste-glasses [23]. Typical waste-glass heat capacities between 50 and 300°C are 0.19 to 0.25 cal g^{-1} $°C^{-1}$, which compares well to values calculated from models based on glass composition, e.g. [24]. Using the theoretical heat capacity, the enthalpy of typical waste glasses at 1150°C is +452 to +474 cal g^{-1}, for a reference temperature of 25°C. Thus, waste-glass composition differences can have a direct effect on melt rates on the order of 5%, and should not be ignored when attempts are made to model the glass melt rate.

Actual waste-glass batch enthalpies do not conform to those of the corresponding glass product. This is especially true when relatively large amounts of redox species are present, as can be seen by comparing Tables 5 and 6. The major feature of the TGA and DSC results of Table 5 is an exothermic reaction at about 300°C. This is attributable to the liquid phase reactions of $NaNO_3$ with NaCOOH or sucrose, with are major constituents of the slurry. See Table 6. In the case of batch SF7, this exotherm is sufficient to provide 65% of the enthalpy required to raise the glass product from room temperature to the final melt temperature. One of the major reasons for slow melting of batch SF-7 is probably increased foam stability because of insufficient amounts of reducing agent to reduce foam persistance [25]. The smaller exotherm for batch SF9 is probably the result of denitration by formic acid during drying. Thus, because of both heat balance and physical chemistry considerations it is essential to model the redox effects if waste-glass melting rate models are to include batch composition variations.

The addition of formic acid to batch SF9 caused a major difference in the ferrous iron content of the partially reacted batches in Figure 4 when compared to batch SF8. There were similar decreases in the $NaNO_3$ content of Table 4, and increases in the spinel of Figure 4. Thus, formic acid is effective in the early elimination of nitrate and reduction of Fe(III) to Fe(II) . In the ratios investigated the sucrose rapidly eliminated $NaNO_3$ during heating, but much of it pyrolyzed. There was much less residual graphite in the SRL feeds and the relative volume of the foam was correspondingly less in Table 3. This may account for part of the melt rate differences in Table 6. The pyrolytic carbon

was consumed when the temperature of the batch exceeded 650°C, during the stage in the melting process where closed pores predominated.

WASTE-GLASS MELTING STAGES AND RESULTING LIMITATIONS

Glass melting stages were assigned to the melting stages of Table 3 based upon comparison of the X-ray diffraction, TGA and DSC data, and the batch composition data of Table 4. This results in the establishment of probable reaction paths for the vitrification of the major waste-glass species. The probable reaction paths are discussed below.

Stage 1- Batch Dried

The slurry pumped to the melter is 40-60% unbound water, which vaporizes when it falls onto the heated cold cap. This occurs during the first 1/4 h that the batch is exposed to temperatures above 650°C. Lid booster heat and reflected heat from vents in the cold cap raise most of the upper surface of the cold cap to the average melter plenum temperature, i.e. about 300°C for melting with no lid heat (SF7 - SF9), and 600 to 850°C for operations with lid booster heaters (SGM3, SGM6).

Partial denitration is the first major chemical reaction. Both formic acid and sucrose are capable of reducing nitric acid under boiling conditions, yielding several gaseous species [26,27]. Loss of chemically bound water is the second major reaction. This begins endothermically, but as the dried salts are heated above their melting points, exothermic reactions dominate, including oxidation of formates and sucrose by nitrates. Such redox reactions are common, and rapidly occur at temperatures above the melting point of the organics and the nitrate salts, which are typically below 350°C. Fused nitrate reactions with carbohydrates rarely reduce the nitrate past nitrite [28] accounting for excess pyrolytic graphite after the elimination of nitrates.

Stage 2- Particles Bonded, Channel Porosity Develops

The melting of formates, nitrates, borates and sucrose occurs during the first 1/2 hour exposure to temperatures above 650°C. The batch particles become weakly bonded, but separate to allow the venting of steam and other gaseous reaction products. The volume of the reacting batch decreases at this point, because of collapsing bridges between particles. Small amounts of pyrolytic carbon were noted by Bonnell, et al, when alkali formates were heated [29]. The amounts evident in Table 4 and Figure 4 suggest that conversion to pyrolytic carbon is enhanced by the presence of low melting point salts.

Stage 3- Porosity Closed, Pores Enlarge, Definition of Minimum Foaming Temperature

It typically takes 1 hour exposure to 650°C, or 1/4 h at 750°C to achieve this stage. As the reactions continue, the volume of the first liquid phase increases, and the increased reaction time and temperature permit more waste and glass forming constituents to dissolve. At this stage Fe_2O_3 begins to dissolve in the glass, and the pyrolytic graphite

begins to be oxidized by the waste, releasing CO_2. In waste batches containing ground glass frit, the frit begins to soften at about 550°C [23], and begins to react with the first liquid. This results in an increase in the liquid viscosity, making it more difficult for gaseous reaction products to escape. At a critical point, the venting of the reaction products essentially ceases, and the batch begins to convert into foam. This is known as the lower foaming limit.

The lower foaming limit depends on the ability of the batch to create a closed pore structure. The viscosity at which this happens can be estimated from the balance of forces. The normal stress condition for a spherical surface in the absence of a pressure difference is

$$\sigma/d + \eta\ V/\ r = 0. \qquad (1)$$

where σ is the surface tension, d characteristic diameter, η viscosity and V radial velocity. The first term represents the capillary force, the second the viscous force. Making an order of magnitude assessment $V/\ r\ \sim V/r$ and $V \sim -r/t$, where t is time, the viscous force is proportional to η/t. Hence,

$$\eta/t \sim \sigma/d. \qquad (2)$$

If σ = 0.3 N/m and d = 100 μm (corresponding to the smallest pore in the isothermal reaction samples), the open pores become closed in t = 30 s (an arbitrary characteristic time) if $\eta = 10^5$ Pa s. SRL nuclear waste glasses reach $\eta = 10^5$ Pa s at about 600°C. This corresponds to the experimental observation that glass begins to foam at about 50°C above the softening point, where $\eta = 10^{6.6}$ PA s [30]. The glass foaming temperature ranges from 620 to 700 °C for calcined waste [13]. With moderate heating rates, foam can exist up to 1000°C, when the the collapse rate becomes higher than gas generation.

Stages 4 and 5- Foam Expands, Determination of Gas Evolution Rate, Foam Density and Porosity, Foam Stability

These stages may be reached in 4 h exposure to 650°C, or 1 h at 750°C. In these stages the silica or frit are still reacting with low melting point liquids, and gas evolution continues from graphite consumption. The resulting gas and high batch viscosity from the combination of increased silica content and low temperature causes the batch to foam to its greatest volume. Heat transfer into the batch at this stage is most difficult, because exothermic carbon reactions are being exhausted at the same time that high porosity causes a minimum in the thermal conductivity of the batch.

Thermodynamic calculations, assuming that the reacting constituents are in their standard states, may not provide correct amounts of gases liberated during heating if

the constituents mutually dissolve, as is the case for nuclear waste glasses [31]. For example, Mn_3O_4 is stable in air at 1150°C, but if it is mixed with glass frit, it evolves 33 cm^3 O_2 at 1150°C, per g Mn_3O_4. For a representative thermodynamic calculation it is necessary to know the activities of the constituents. In addition, the gas evolution rate is affected by reaction kinetics. Alternatively the gas evolution rate can be determined thermoanalytically. However, the small size of thermoanalytical samples makes them sensitive to the surrounding atmosphere, whereas the batch in the cold cap of a melter is essentially exposed only to its own gases.

The results of thermogravimetric analysis performed by Lucktong [32], of a simulated SRL "sludge only" glass batch containing 70% frit, are shown in Table 7. The results are comparable to those of the SRL "Coupled" process in Table 3. Lucktong's results can also be compared with more detailed data obtained for calcined waste by Slates, et al, [33] shown in Table 8. The differences between Tables 7 and 8 indicate that some reactions (such as those evolving CO_2) occur at lower temperatures if the waste is mixed with glass frit, and that the nuclear waste glass from hydrated waste evolves a substantially larger amount of gas above 700°C than does glass from calcined waste.

The fractional mass loss, β, shown in Table 7, is the mass of gas evolved from a unit mass of waste glass. The gas-to-glass volume ratio, v, was obtained by

$$v = \beta \rho_G RT/MP \qquad (3)$$

where ρ_G is the glass density, R gas constant, T temperature, M molecular mass of gas, and P pressure. The values of v shown in Table 7 are based on the assumption that the gas is oxygen, the batch contains 30 mass % of dry nuclear waste, and P ~ 10^5 Pa. The total volume of the liberated gas is 43 times larger than that of the glass.

The density of foam, ρ_F, and its porosity, ε, are related to the volume of pores per unit volume of glass, V_p, by

$$\rho_F = (V_P + 1)^{-1} \rho_G \qquad (4)$$

where V_P is the volume of pores per unit volume of glass and ρ_G is the glass density. The foam porosity is

$$\varepsilon = 1 - \rho_F/\rho_G \qquad (5)$$

or, by (4),

$$\varepsilon = (1 + V_P^{-1})^{-1} \qquad (6)$$

Based on Table 7 if all the gas liberated between 600 and 1000°C was retained as porosity then the foam density would be 96 kg m^{-3} and foam porosity 96%.

Such extremely high porosity was seen in samples SF8 and SF9, made from batch chemicals (Table 3). However, experiments with foam glass show that it is difficult to maintain density lower than 200 kg m^{-3} [30]. The larger foam volumes of the SF series are attributable to the unusual redox reactions discussed earlier. The experiments with SG3, SG6 and earlier experiments with SRL "sludge only" glasses never showed foam volumes larger than 4 volumes of the bubble free glass [13,32]. Thus, $V_p = 3$ is a reasonable representative value for the coalescence limit of these foams. This limit is reached before spherical bubbles can grow into a honeycomb cell structure [13,34,35]. The corresponding amount of gas required to produce the foam is liberated by a temperature increase of only 6°C in the interval from 700 to 800 °C. The corresponding minimum foam density and maximum porosity are $\rho_F = 630$ kg m^{-3} and $\varepsilon = 0.75$.

It is inevitable that the nuclear waste glass becomes foam during its passage through the melter, because the amount of gas evolved from heating nuclear waste during the vitrification process exceeds many times that which can be retained in foam. The large gas generation rate will maintain the foam density at its minimum level within the whole temperature interval between 700 and 1000°C. The excess gas will leave through vent holes. If the gas cannot make its way up through the foam and escape through the porous upper layer, then pressure will increase until the gas can lift or break up the the upper layer.Gas pushing up also destabilizes the process by producing surges in the off gas evolution rate, and by causing dicontinuities in the conduction of heat into the reacting batch. A combination of glass convection currents and the gas pressure may also push the relatively low viscosity foam to the furnace side walls, where the foam may cool and stabilize. Such foam has been observed, slowing the melting process.

Foam stability and the foaming temperature range are also affected by the the presence of molten salts which make a separated liquid phase of low viscosity and low surface tension. The addition of sodium sulfate and sodium chloride is known to be ffective in accelerating foam collapse and melt rate [36].

Not fully understood is Goldman's finding that waste glasses with Fe(II)/ Fe(III) ratios greater than 0.05 have less persistent foam than the same glasses fully oxidized [25]. The ability to convert Fe(III) to Fe(II) and Mn(IV) to Mn(II) could result in surface tension, viscosity, and surface diffusion differences. Differences could also be the result of variations in the water or carbonate contents.

Since it is likely that a foam layer will be formed in nuclear waste glass melters, limits are necessary to assure that the foam will eventually collapse as the material is heated to the melting temperature, and a relatively bubble-free melt will be produced. Conditions are estimated below which will guarantee that each batch particle moving through the melter is provided a sufficient time for foam collapsing and bubble removal.

Stages 6-10 Porosity Reduced and Eliminated- Definition of Bubble Removal Limit

It requires 2 h at 850°C or 1/2 h at 950°C to reach the earliest of these stages. Final porosity elimination requires about 2 h at 1150°C, based on the crucible tests shown in Figure 3. During these stages the glass becomes homogeneous, developing its final durability, dissolves the remaining refractory species such as SiO_2 and spinel, and eliminates porosity. The condition for bubble-free melt is that the pull velocity, N/ρ_G, where N is the glass production rate per surface area of batch-melt interface, must be smaller than the velocity at which bubbles ascend by Stokes law,

$$u_S = 2/9\ \rho_G g r^2/\eta \qquad (7)$$

Therefore, the condition for bubble-free melt is

$$N < 2/9\ \rho_G^2 r^2 g/\eta \qquad (8)$$

For $r = 400\ \mu m$, a radius similar to those seen in the isothermal samples during the later stages of melting, and $N = 72\ kg\ m^{-2}\ h^{-1}$, the bubbles will move upwards if $\eta < 100$ Pa s. This condition is commonly satisfied in nuclear waste glass melting.

During the passage of the material through the foam layer the foam structure becomes unstable when the gravity driven drainage of the melt between bubbles becomes faster than the velocity N/ρ_F. The gravity driven velocity is proportional to $gd^2\rho_G/\eta$, where d is the distance between bubbles. Since $\rho_F = (1-\varepsilon)\ \rho_G$, the drainage limit for viscosity is

$$N < (1-\varepsilon) g d^2 \rho_G^2/\eta \qquad (9)$$

Taking $d = 100\ \mu m$, $N = 2 \times 10^{-2}\ kg\ m^{-2} s^{-1}$ and $\varepsilon = 0.75$ as conservative values, this inequality yields $\eta < 45$ Pa s. Accordingly, the melting viscosity should be of the order of 10 Pa s or less. This value is lower than that to guarantee the bubble removal. Therefore, the foam drainage inequality (9) is more restrictive than the bubble removal inequality (8).

Since foam collapse velocity may be affected by coalescence to an even greater degree than by gravity drainage [37], it is sufficient that the velocity N/ρ_F is lower than the foam collapsing velocity, u_F. Hence, the charging rate is limited by the inequality

$$N < \rho_F u_F \qquad (10)$$

The foam collapsing velocity can be defined as the rate at which the foam layer thickness decreases when gas supply is stopped. This velocity was measured in fiber glass by Gerrard and Smith [38]. They created foam by reducing pressure, then increased the pressure and measured the time taken for collapse in the range of η between 10 and 400 Pa s. Assuming a linear decrease of foam height with time, Gerrard and Smith calculated u_F, plotted it against viscosity, and found a linear decrease of u_F with log η. Consequently,

$$u_F = u_O(1-A \ln [\eta/\eta_1]) \qquad (11)$$

where u_O and A are constants. The respective constant values, evaluated from Gerrard and Smith's data, are $u_O = 7.2$ m h^{-1}, A = 0.11, and $\eta_1 = 1$ Pa s.

The foam collapsing rate was not found by Gerrard and Smith to be proprotional to η^{-1}, as it would be expected if foam collapsing is controlled by flow. There is also a question whether the linear relationship between u_O and ln η can be applied to nuclear waste glasses, and how far it can be extrapolated beyond the experimentally verified range. Assuming that A =0.11 for nuclear waste glass, the value of u_O was evaluated from Ahn's results [13], confirmed by the waste glasses in Figure 3, that at 1000°C the collapse rate is 0.09 m h^{-1}. This leads to $u_O = 0.12$ m h^{-1}.

Table 9 shows some values of $N_C = \rho_F u_F$, the critical charging rate, for different values of η and ρ_F. For example, if $\rho_F = 0.6$ g cm^{-3}, N cannot be higher than 54 kg m^{-2} h^{-1} if the viscosity is 10 Pas, but it can approach 72 kg m^{-2} h^{-1} if the viscosity is 1 Pa s. If the viscosity is 10^3 Pa s, then N cannot exceed 18 kg m^{-2} h^{-1}. Higher charging rates will result in unstable melting. Comparison of inequalities (14) and (17) indicates that with η < 1000 Pa s the melting rate will indeed be limited by foam collapsing, rather than bubble removal.

If the linear relationship between u_F and ln η can be extrapolated to higher viscosities than 400 Pa s, the foam freezes at $\eta = 8.9 \times 10^3$ Pa s, which corresponds to 620°C for high iron nuclear waste glass. This implies that the presence of low viscosity molten salts, such as sulfates and borates is desireable to increase melt rates.

The viscosity term in equation (11) causes less than 25% reduction in the melting rate if η = 10 Pa s. Therefore, from the point-of-view of glass melting, foam can be considered as relatively persistent if the viscosity is 10 Pa s < η .

For given ρ_F and N, the melting viscosity must be smaller than

$$\eta < \eta_0 \exp A^{-1}(1 - N/\rho_F u_O) \qquad (12)$$

This inequality indicates that the critical viscosity for foam collapse is determined by the melting rate and the foam density. Using the above given values of u_O and A and assuming that $\rho_F = 0.63$ g cm^{-3}, for a melting rate of 36 kg m^{-2} h^{-1} the critical viscosity is 110 Pa s.

Estimation of Melt Rate Based on Foam Modeling

Table 9 shows the maximum melting rate allowed by steady state melting of a foaming batch. However, the actual melting rate can be limited by the heat flux to the reacting layer of batch (cold cap) through the foam layer. The heat flux needed for batch melting is

$$q = Q_U N \qquad (13)$$

where Q_U is the sum of the reaction heats from Table 5, plus the sum of the sensible heats of the products (which can be estimated from heat capacities of the glass product for endothermic melts), minus the heat flux entering the cold cap from lid heaters. Since this heat must be conducted through the foam layer, it can be expressed as

$$Q_U N = k\Delta T/h \qquad (14)$$

where k is the foam thermal conductivity, ΔT the temperature difference across the foam layer, and h the foam layer thickness. The variables Q_U, ΔT, and k are nearly constant for a given batch composition, so it follows from (14) that the foam layer thickness decreases as the melting rate increases. Thermocouple probes of cold caps have not been sensitive enough to determine this difference, but sensitive arrays of thermocouples should be effective in determining the onset of unstable foaming, based upon (14). To predict both N and h separately, a more detailed analysis is developed below.

Energy Equation For Foam Layer

The foam layer is part of the reacting layer, for which the energy equation assumes the form [36]

$$kT'' + cNT' - \rho Q\dot{\xi} = 0 \qquad (15)$$

where c is the heat capacity, Q the reaction heat within the foam layer, ξ degree of conversion, prime derivatives are with respect to vertical distance and dot material derivatives are with respect to time.

Assuming that ξ changes linearly with time ($\ddot{\xi} = 0$) and using the relation $\xi' = -\dot{\xi}\rho/N$, equation (15) becomes

$$k\rho\dot{\xi}N^{-2}T_{\xi\xi} - cT_{\xi} - Q = 0 \qquad (16)$$

where $T_{\xi} = \partial T/\partial\xi$. If the reaction starts at $T(0) = T_O$ and ends at $T(h) = T_1$, the solution of equation (16) is

$$T = T_O + (T_1 - T_O + Q/c)\,[\exp(cN^2\xi/k\rho\dot{\xi}) - 1]/[\exp(cN^2/k\rho\dot{\xi}) - 1] - \xi Q/c \qquad (17)$$

Equation (17) represents the temperature distribution within the foam layer with respect to the degree of conversion. It was assumed that the degree of conversion is a linear function of time, and the velocity at which the material moves within the foam layer is constant (because its density is constant). The temperatures T_O and T_1 are the lower and upper foaming temperatures discussed above.

Calculation of Waste-Glass Melting Rate

Experimental melting rates using simulated SRS "sludge only" waste glass were in the range 14 to 36 kg m^{-2} h^{-1}, limited by cold cap bridging. When this is combined with the observation that melter cold caps are about 5 to 10 cm thick, it is concluded that the average time for a unit of melter batch to be converted to bubble free glass is 0.9 to 4.4 h, if it is assumed that the volume fraction porosity is 0.75 .

The heat flux from the foam layer to the batch blanket above it can now be determined. Since $q = -kT'$, equation (13) and a transformation of variables yields

$$k\rho\dot{\xi}T_{\xi}(0) = N^2Q_U \qquad (18)$$

Expressing $T_{\xi}(0)$ from equation (17) yields:

$$(1 + c\Delta T/Q)\,(\exp(cN^2/k\rho\dot{\xi}) - 1)^{-1} = Q_U/Q + k\rho\dot{\xi}/cN^2 \qquad (19)$$

where $\Delta T = T_1 - T_O$. Using dimensionless variables $\bar{N} = (c/k\rho\dot{\xi})^{1/2}N$, $\bar{T} = c\,\Delta T/Q_U$, and $\bar{Q} = Q/Q_U$, equation (19) can be rewritten as

$$(1 + \bar{Q}/\bar{N}^2)(\exp \bar{N}^2 - 1) = \bar{T} + \bar{Q} \qquad (20)$$

Equations (19) and (20) determine the melting rate. They considerably simplify if $\bar{Q}$ and $\bar{N} << 1$. Then $\bar{N}^2 = \bar{T}$, or

$$N^2 = k\rho\dot{\xi}\Delta T/Q_U \qquad (21)$$

If $\bar{Q}$ is small so that $\bar{Q}/\bar{N}^2 << 1$ and $\bar{Q} << \bar{T}$, then equation (20) simplifies to

$$\bar{N}^2 = \ln(1 + \bar{T}) \qquad (22)$$

Thermal conductivity depends on porosity by

$$k = \varepsilon k_r + (1 - \varepsilon)k_S \qquad (23)$$

where the subscript r stands for the radiative contribution through pores and s for conduction through the condensed phase. The radiative contribution can be omitted for pore sizes smaller than 1mm because of the relatively low foaming temperatures discussed above. When the relation $\varepsilon = 1-\rho_F/\rho_G$ is used for density, equation (21) becomes

$$N = (1 - \varepsilon)(k_S\rho_G\dot{\xi}\Delta T/Q_U)^{1/2} \qquad (24)$$

Similarly, equation (22) assumes the form

$$N = (1- \varepsilon)[k_S\rho_G\dot{\xi}c^{-1}\ln(1 + c\Delta T/Q_U)]^{1/2} \qquad (25)$$

Hence, the melting rate is directly proportional to the melt volume fraction, $1 - \varepsilon$, within the foam layer. Thus, any chemical or mechanical action which reduces the void fraction in the cold cap can be expected to increase the melt rate.

This result is not restricted by any major simplifying assumptions. According to (20), $N = (k\rho\dot{\xi}/c)^{1/2} f(\bar{T}, \bar{Q})$ and thus, since $k \sim (1 - \varepsilon)k_s$ and $\rho = (1 - \varepsilon)\rho_G$, so $N = (1 - \varepsilon)(k_s \rho_G\dot{\xi}/c)^{1/2} f(\bar{T}, \bar{Q})$, where the function $f(\bar{T}, \bar{Q})$ is the solution of equation (20).

Equations (19), (24), and (25) relate melting rate to the batch conversion kinetics. Combination of these equations with a simplified heat flow model, such as that by

Lee [12] should provide a reliable model which adequately considers both melter operating conditions, and batch chemical properties.

The thermal diffusivity and heat capacity of nuclear waste batches up to 400°C are [23] $\alpha = 4 \times 10^{-3} cm^2\ s^{-1}$ and $c = 0.24$ kcal $kg^{-1}\ °C^{-1}$, and thus $k_s = 2.39 \times 10^{-3}$ cal $cm^{-1}\ °C^{-1}$. At temperatures 700-1000°C, k_s and c have higher values because the batch is virtually all molten. The melting heat can be based on DSC as in Table 5. Therefore, the values adapted by Routt [10], i.e., $k = 1.05 \times 10^{-2}$ cal $cm^{-1}\ °C^{-1}$ and $c = 0.33$ cal $g^{-1}\ °C^{-1}$ are used in the following calculations, with $Q_u = 143$ cal g^{-1}. Foaming temperature range can be assessed at $\Delta T = 300$ K [32]. The conversion rate from DSC measurements is $\dot{\xi} = 0.72\ h^{-1}$.

Using these data, $\bar{T} = 0.7$ and, by (22), $\bar{N} = 0.73$, so $N = 104\ (1 - \varepsilon)$ kg $m^{-2}\ h^{-1}$. For $\varepsilon = 0.75$, the melting rate is 26 kg $m^{-2}\ h^{-1}$. Using Ahn's data [2] the foam porosity is 0.64 which results in the melting rate 37 kg $m^{-2}\ h^{-1}$. Repeating this calculation with $Q_u = 98$ cal g^{-1}, yields $N = 30$ kg $m^{-2}\ h^{-1}$ ($\varepsilon = 0.75$) or 43 kg $m^{-2}\ h^{-1}$ ($\varepsilon = 0.64$). All these values are within the range of experimental values and limiting values shown in Table 9. Since the radiative contribution within the pores was neglected, the values of N may be underestimated.

Estimation of Foam Layer Thickness

Eliminating N from equations (14) and (19), yields an equation relating the foam layer thickness to its properties. In a normalized form it becomes

$$(1 + \bar{Q}\ \bar{h}^2)(\exp\ \bar{h}^{-2} - 1) = \bar{T} - \bar{Q} \qquad (26)$$

where $\bar{h} = (\rho\xi/kc)^{1/2}(\Delta T h/Q_U)$. If $\bar{Q} << \bar{T}$ and $\bar{Q} << \bar{N}^2$, equation (26) simplifies so that h can be expressed as

$$h = (\Delta T/Q_U)\ (ck_S/\rho_G\xi)^{1/2}[\ln(1+c\Delta T/Q_U)]^{-1/2} \qquad (27)$$

where the relation $k/\rho = k_s/\rho_G$ was used.

Equations (26) and (27) imply that h is independent of porosity, which is not an obvious result. However, an inspection of equation (14) shows that if both N and k are proportional to $1 - \varepsilon$, h must be independent of ε. The value of ε determines whether the layer is foam or just a bubbly melt. If ε is very low, the layer in question becomes a part of the melt and is subject to convection.

Using the values of properties given earlier, the foam layer thickness can be calculated. Equation (27) yields h = 7.6 cm, in good agreement with observed values. A foam layer of this thickness may be mechanically unstable. The weight of the cold cap may push the foam towards the furnace walls and along the walls upwards, which may lead to bridging. Therefore, it is desireable that the foam density is high. The foam layer thickness decreases as ΔT increases. This means that if the temperature interval during which gases are evolved is reduced, the foam layer will be thinner, for example, if ΔT is reduced from 300 to 100 C, h = 4 cm.

Agitation to Increase Melt Rate

Given a foam thickness of 7.6 cm, an unagitated melt rate of 35 kg m^{-2} h^{-1}, and an average foam density of 0.6 g cm^{-3}, the average velocity through the cold cap is 5.8 cm h^{-1} and the average cold cap residence time is 1.3 h. This residence time is required in conventional melters to convert the batch to glass. The melt rate per unit surface area can be increased by either decreasing the time required to transfer heat into the batch, or by mechanically accumulating the cold cap to a greater depth. Decreasing time to transfer the heat can be effected by decreasing the heat transfer distance, venting gases causing porosity, and by renewal of glass in contact with the reacting batch.

If a 10 fold increase is to be accomplished by an increase in heat transfer rate into the batch, then the average residence time to heat a portion of the batch must be decreased to 0.13 h . The integral of Fick's second law requires that the characteristic heat transfer distance be reduced by a factor of the square root of 10 to accomplish equivalent heating in the reduced time. Based upon two sided heating of a 7.6 cm thick cold cap, this can be accomplished by preventing the formation of islands of cold material larger than about 1 cm diameter on the melt's surface. To stabilize these small islands, and preclude their coalescence, it is necessary control the distance between the islands, or to renew the melt between islands to compensate for heat absorbtion. It is reasonable to assume that heat renewal can be accomplished if the surface is sheared 20 times during the 0.13 h period. This is equivalent to a shear rate of 150 h^{-1}. Higher average shear rates might be necessary to shear relatively stagnant areas of the melt at this minimum rate.

Meeting the minimum residence time to heat the batch is not sufficient to guarantee chemical homogeity of the glass. However, the leach test results of Figure 5 demonstrate that a hold time of two hours at 950°C, or 1 hour at 1150°C develops glass durability comparable to 4 hours at 1150°C.

Agitated Melter Testing

The measured slurry melt rates of 155 kg m^{-2} h^{-1} with agitation (32 lb ft^{-2} h^{-1}), and 19.5 kg m^{-2} h^{-1} (4.0 lb ft^{-2} h^{-1}) without agitation demonstrate an increased melt rate factor of 8, comparable to the corresponding factor of 12.6 calculated from Richards' tests with commercial glass [20]. The demonstrated melt rate was limited by the ability of the agitation to disperse the slurry as it was sheared by the underlying foam. Estimated electrode current densities indicate that an additional factor of 2 increase is possible before electrode current is limiting melt rate. It is therefore concluded that slurry fed waste-glass melt rates of about 290 kg m^{-2} h^{-1} (60 lb ft^{-2} h^{-1}) are possible through design optimization.

SUMMARY AND CONCLUSIONS

The major chemical compounds which form as intermediate products in radioactive waste vitrification have been identified, and initial efforts made at quantifying the temperatures, rates, extent, and sequence of reactions. Based upon this analysis, modeling of waste glass melter production rates should concentrate on the determination of effective heat capacity of batch vitrification, which is a function of waste dehydration, redox reactions, and the final glass composition. Relatively high melt rates of wastes containing both reducing agents and oxidizing agents can be attributed to the exothermic reactions which occur.

Waste glass-melter size and residence times required by glass quality are much smaller than those used in current practice. Melter residence times shorter than 4 hours, at tempertures lower than 1050 °C are sufficient to develop durability similar to that of existing melters operating at 1150 °C, with residence times over 10 times longer.

A bubble removal limit, which requires that the downward vertical velocity of melt is lower than the velocity of the ascending bubbles, and a foam collapsing limit, are defined for waste glass melters, and estimated based upon thermochemical measurements. At melting temperatures used for nuclear waste glasses, the foam collapsing limit imposes the greatest restriction on the glass production rate. The critical melting rate, above which the steady state melting is upset, is determined by the melting viscosity, which must be low enough to allow rapid collapsing of foam. Therefore, it is desireable to operate waste glass melters at constant melting viscosity, rather than constant nominal temperature.

The total gas produced during waste vitrification exceeds many times the amount needed to create foam. The foam layer thickness has therefore been derived in a manner unrelated to the total amount of gas produced at any temperature. The amount of foam is restricted by the viscosity, and the minimum foam density. Below the minimum foam density, excess gas escapes through the vent holes, and foam collapses. However, if the melting viscosity is too high, so that foam collapses too slowly, the melter produces foam instead of bubble free melt. Then a steady state cannot be attained unless the charging rate is extremely low.

Foaming during waste glass melting can be minimized through the minimization of the gas evolved, or by minimizing the viscosity in the critical temperature range. The foaming range is primarily a function of viscosity, since viscosity relates the relative rates of competing foam production and foam destruction processes. Through the use of controlled reducing agent, alkali and boron addition to waste, and corresponding removal of these compounds from glass forming frits, it is possible for the DWPF to produce nearly fully oxidized glasses at high production rates, without excessive foaming, and without changing the final composition and properties of the glass produced. This is accomplished by the use of balanced amounts of reducing agent and oxidizing agent to support redox reactions at critical intermediate stages of the melting process.

West Valley waste is high in nitrate content, and therefore produces glass in the high oxygen fugacity region of waste glass production. WV work has emphasized the suppression of glass foaming which results when fully oxidized transition metals are reduced during dissolution in glass. Through the use of controlled amounts of sucrose and formic acid as carbothermic reducing agents, the SF7 through SF9 runs marked the first WVDP melter test runs in which required melting rates were demonstrated. Through this technique, sustained feeding campaigns were achieved without interruption by reboil and foaming excursions.

Glass melt studies support Goldman's conclusion that waste glass foam is least persistant when final glass is sufficiently reducing that Fe(II)/(III) ratios are above 0.05 .

Melter size can be minimized when the reacting batch is sheared. Shearing renews heat transfered to the reacting melt, and maintains short heat transfer distances in the reacting batch. This leads to rapid heating of the feed, andenhanced conversion rates. A new class of waste glass melters has been designed, and proof of concept tests completed on simulated High Level Radioactive Waste slurry. Melt rates have exceeded 155 kg m^{-2} h^{-1} with slurry feeds (32 lb ft^{-2} h^{-1}), and 229 kg kg m^{-2} h^{-1} with dry feed (47 lb ft^{-2} h^{-1}) . This is about 8 times the melt rate possible in conventional waste-glass melters of the same size.

ACKNOWLEDGEMENTS

The information contained in this article was developed during the course of work under contracts No. DE-AC09-76SR00001 and DE-AC07-81NE44139 with the U.S. Department of Energy. Dr. P.K. Smith conducted the X-ray diffraction studies. Development and operation of the agitated melter was a joint program between Mr. Ray Richards, Associated Technical Consultants, Toledo O, and SRL. Inconel 690 is a trademark of Inco Alloys International, Huntington, WV.

REFERENCES

[1] C. Chapman, J. M. Pope, S. M. Barnes,"Electric Melting of Nuclear Waste Glasses: State of the Art", J. Non-Cryst. S. 84 (1986) 226-240.

[2] M.D. Boersma, and J. L. Mahoney,"Glass Making Technology for High-Level Nuclear Waste", Proc. Symp. AIChE, Boston MA, August,1986.

[3] J.L. McElroy, W.J. Bjorklund and W.F. Bonner,"Waste Vitrification: A Historical Perspective", The Treatment and Handling of Radioactive Wastes, Springer-Verlag (1982) 171-177.

[4] Y.S. Tang and J.H. Saling, Radioactive Waste Management, Hemisphere Publ. (1990).

[5] C.C. Chapman,"Design Preferences for a Slurry-Fed Ceramic Melter,...", Proc. 2nd Int. Symp. Ceramics in Nucl. Waste Man., 8 (Am. Cer. Soc. 1983) 159.

[6] J.P. Giraud, J.P. Conard, and P.M. Saverot,"Conceptual Design for Vitrification at West Valley,...", Proc. 2nd Int. Symp. Ceramics in Nucl. Waste Man., 8 (Am. Cer. Soc. 1983) 134.

[7] D. F. Bickford, R.C. Propst and M. J. Plodinec,"Control of Radioactive Waste Glass Melters Part III: Glass Electrical Stability", Advances in the Fusion of Glass (Am. Cer. Soc. 1988) 19.1-19.17 .

[8] D. F. Bickford, R. S. Ondrejcin and L. Salley,"High Temperature Materials for Radioactive Waste Incineration and Vitrification", Advances in Ceramics, Vol 20 (1987) 65-78.

[9] K. R. Routt, "Theoretical Predictions for Continuous Slurry Feeding of a Glass Melter", Mat. Res. Soc. Symp. Proc. Vol 15 (1983) 623-630.

[10] K. R. Routt,"Physical Modeling of a Glass Melter Designed for Vitrification of Defense Waste", G.G. Wicks And W. Ross, Ed., Advances in Ceramics, Vol 8 (1984) 536-549.

[11] D. W. Pepper,"Recirculation Within a Glass Mixture Subjected to External and Resistive Heating", Fourth Inter. Conf. Num. Meth. in Laminar and Turb. Flow, Swansea UK, July 1985.

[12] L.-M. Lee,"Prediction of Waste Glass Melt Rates", Waste Management '87, Vol 1, Am. Nucl. Soc., 591-593.

[13] J.S. Ahn and P. Hrma,"The Effect of Heat Treatment on Foaming of Simulated Nuclear Waste in a Borosilicate Glass Melt", Advances in Ceramics, Vol 20 (1986) 181-190.

[14] "Heat Flow Calibration of Differential Scanning Calorimeters", ASTM E 968-83 (1983).

[15] "Temperature Calibration of Differential Scanning Calorimeters and Differential Thermal Analyzers," ASTM E 967-83 (1983).

[16] E.W. Baumann, C.J. Coleman, D.G. Karraker, and W.H. Scott,"Colorimetric Determination of Fe(II)/Fe(III) Ratio in Glass", SRL Report DP-MS-87-18, Aug. 1987.

[17] C.M. Jantzen and D.F. Bickford,"Leaching of Devitrified Glass Containing Simulated SRP Waste", Mat. Res. Soc. Symp. Proc. Vol. 44 (1985)135-145.

[18] D.F. Bickford,"Advanced Waste-Glass Melters", Am. Cer. Soc., Dallas TX, April 1990.

[19] R.S. Richards," Small High-Speed Glass Melter for Waste Vitrification", Am. Cer. Soc., Dallas TX, April 1990.

[20] R.S. Richards,"Rapid Glass Melting and Refining System", Advances in the Fusion of Glass (Am. Cer. Soc. 1988) 50.1-50.11 .

[21] D.F. Bickford and C.M. Jantzen,"Devitrification Behavior of SRL Defense Waste Glass", Mat. Res. Soc. Symp. Proc. Vol 26 (1984) 557-566.

[22] D.F. Bickford and C.M. Jantzen,"Devitrification of Defense Nuclear Waste Glasses: Role of Melt Insolubles", J. Non-Cryst. Sol. 84 (1986) 299-307.

[23] L. D. Pye, The Physical and Thermal Properties of Simulated Nuclear Waste Glasses and Their Melts" D. F. Bickford ed.,"Measured Physical Properties of Simulated DWPF WasteGlasses", OSTI/DPST-85-397, March 1985.

[24] M.A. Matveev, G.M. Matveev, and B.N. Frenkel,"Calculation and Control of Electrical, Optical and Thermal Properties of Glass", (Ordentlich, Holon Israel, 1975) 50.

[25] D. S. Goldman,"Melt Foaming, Foam Stability and Redox in Nuclear Waste Vitrification", J. Non-Crystalline Solids 84 (1986) 292-298.

[26] R.F. Bradley and C.B. Goodlett,"Denitration of Nitric Acid Solutions by Formic Acid", DP-1299, June 1972.

[27] L.A. Bray,"Denitration of Purex Wastes with Sugar", HW-76973 REV, 1963.

[28] J.A. Conkling, Chemistry of Pyrotechnics, (Marcel Dekker, Inc., 1985) 43.

[29] D.W. Bonnell, E.R. Plante, and J.W. Hastie," Vaporization of Simulated Nuclear Waste Glass", J. Non-Cryst. Sol. 84 (1986) 268-275.

[30] S. Kose and G. Bayer,"Foam Formation and Foam Properties in the System Waste Glass-SiC", Glastech. Ber. 55 (1982) 151-160.

[31] D. F. Bickford and R. B. Diemer, Jr.,"Redox Control of Electric Melters with Complex Feed Compositions: Part I", Journal of Non-Crystalline Solids 84 (1986) 276-284.

[32a] C. Lucktong, P. Hrma, and A. R. Cooper,"Foaming in Glass Melt Induced by Dissolution Accompanied by Chemical Reaction", Case-Western Reserve University, 1985.

[32b] C. Lucktong,"Direct Observations of Foaming in Molten Glass", M.S. Thesis, Case Western Reserve Univ., 1987.

[32c] C. Lucktong, and P. Hrma,"Oxygen Evolution During MnO and Mn3O4 Dissolution in a Borosilicate Melt", J. Am. Cer. Soc. 71 [5] (1988) 323-328.

[33] R. V. Slates, W. C. Mosley, Jr., B. Tiffany, and J. A. Stone, "Physical and Chemical Characterization of Synthetic Calcined Sludge", DP-1541, March, 1982.

[34] C. Lucktong and P. Hrma,"Foaming in Glass Melt Induced by Dissolution Accompanied by Chemical Reaction", Case Western Reserve Univ., Oct. 1985.

[35] C. Lucktong and P. Hrma,"The Dissolution of Solids in Melts Accompanied by Gas Evolution",Case Western Reserve Univ., Jan. 1985.

[36] H. Pieper,"Batch Feeding into All-Electrical Tanks", Glastech. Ber. 52, [11] 229-236 (1979).

[37] A. Monsalve and R. S. Schechter, "The Stability of Foams: Dependence of Observation on the Bubble Size Distribution", J. Colloid Interface Sci. 97[2], 327-335 (1985).

[38] A. H. Gerrard and I. H. Smith, "Laboratory Techniques for Studying Foam Formation and Stability in Glass Melting", XIII International Congress on Glass, Glastech Ber. 56 K, Vol. 1, 13-18 (1983).

[39] P. Hrma, "Thermodynamics of Batch Melting," Glastech Ber. 55 [7] 138-150 (1982).

TABLE 1:
DEMONSTRATION WASTE-GLASS COMPOSITIONS

		SAVANNAH RIVER LAB.		WEST VALLEY DEMONSTRATION PROJ.		
SPECIE (WT% OF GLASS)	E GLASS	SGM3	SGM6	SF7	SF8	SF9
Al_2O_3	12-14	5.51	5.50	3.13	2.99	6.13
BaO	0	0	0	0.06	0.33	0.15
B_2O_3	5-10	10.89*	8.77#	9.90	11.04	10.06
CaO	16-25	1.90	1.70	0.61	0.58	0.40
Ce_2O_3	0	0	0	0.23	0.22	0.10
Cr_2O_3	0	0.15	0.15	0.24	0.22	0.17
Cs_2O	0	0.10	0.09	0.11	0.10	0.09
CuO	0	0.36	0.41	0	0	0
Fe_2O_3	0-0.8	13.76	14.02	11.75	11.22	11.60
K_2O	0-1	3.41	2.49	4.78	5.43	3.87
La_2O_3	0	0	0	0.12	0.11	0.05
Li_2O	0	2.97*	2.87#	2.98	3.08	3.00
MgO	0-5	0.59*	1.15#	1.26	1.21	1.25
MnO	0	2.69	3.01	1.43	1.37	1.13
Na_2O	0-1	10.74*	12.46#	10.90	11.97	11.32
NiO	0	1.30	1.17	0.71	0.68	0.10
Nd_2O_3	0	0	0	0	0	0.10
P_2O_5	0	0.05	0.05	2.54	2.42	2.41
RuO_2	0	0.3	0.3	0.07	0.02	0.02
SiO_2	52-56	44.64*	45.46#	44.46	42.48	43.88
Sm_2O_3	0	0	0	0	0	0.02
SrO	0	0.04	0.04	0.13	0.12	0.05
TiO_2	0-2	0.92	0.67	0.99	0.94	0.99
Y_2O_3	0	0	0	0.02	0.02	0.02
ZrO_2	0	0	0	3.13	2.99	2.27
$SO_3^=$	0	0.35	0.30	0.13	0.12	0.29
Cl^-	0	0.30	0.30	0	0	0
F^-	0-1	0	0	0	0	0

* ADDED AS SRL FRIT 200.
# ADDED AS SRL FRIT 200, PLUS 2.3 WT% AS COLLOIDAL SiO_2 FOR COMPOSITION ADJUSTMENT.
OTHER SRL BATCH COMPONENTS ADDED AS HYDRATES STABLE AT pH 12, THEN FORMATED.
WVDP GLASS BATCHED FROM COLLOIDAL SiO_2, BORIC ACID, NITRATES , FORMIC ACID AND SUCROSE.

TABLE 2:
SRL FRIT COMPOSITIONS, wt%

USE	SLUDGE-ONLY GLASS		COUPLED-WASTE GLASS	
DESIGNATION	131	165	200	202
SiO_2	57.9	68.0	70.0	77.0
Na_2O	17.7	13.0	11.0	6.0
Li_2O	5.7	7.0	5.0	7.0
B_2O_3	14.7	10.0	12.0	8.0
MgO	2.0	1.0	2.0	2.0
TiO_2	1.0	0	0	0
La_2O_3	0.5	0	0	0
ZrO_2	0.5	1.0	0	0

TABLE 3:
RELATIVE VOLUMES* OF GLASS BATCH
DURING WASTE-GLASS MELTING

SAMPLE		SRL	WVDP
REACTION STAGE			
1:	BATCH DRIED	3.0	5.1
2:	PARTICLES BONDED, CHANNEL POROSITY DEVELOPS	2.0	5.4
3:	POROSITY CLOSED, PORES ENLARGE	2.0	3.8
4:	SMALL, SPHERICAL PORES DOMINANT	1.8	13
5:	LARGE PORES DOMINANT	2.3	23
6:	LARGE PORES COLLAPSING	1.6	5.1
7:	LARGE PORES ELIMINATED	1.3	3.0
8:	SMALL PORES RISE, AND BEGIN COLLAPSING	1.2	3.6
9:	POROSITY VIRTUALLY ELIMINATED	1.0	1.8
10:	POROSITY ELIMINATED, GLASS DRAINED FROM CRUCIBLE WALL	1.0	1.0

*VOLUMES ARE RELATIVE TO THOSE OF THE FINAL GLASS, BASED UPON FOAM HEIGHT.

TABLE 4
RELATIVE AREAS OF X-RAY DIFFRACTION PEAKS
IN WASTE-GLASS BATCH SAMPLES HEATED 4 HOURS AT 400°C

SAMPLE	SAVANNAH RIVER		WEST VALLEY	
PEAK	SGM3	SGM6	SF8	SF9
SPINEL (440)	0	0.2	0	0.1
Fe_2O_3 (104)	4.0	4.2	1.3	2.3
GRAPHITE (002)	0.4	3.0	6.5	7.8
SiO_2 (100)	---	0.8	2.5	3.1
$NaNO_3$ (104)	0.4	0.8	2.9	2.0

TABLE 5

THERMAL GRAVIMETRIC ANALYSIS AND DIFFERENTIAL SCANNING CALORIMETRY OF WASTE GLASS BATCHES

Sample	Temp. Range, °C	Fraction Mass Loss	DSC Peak °C	ΔH, cal/g
Formated Sludge	80-245	0.13	160+	+43
	245-420	0.16	292-, 355-	-68
	420-960	0.09	None	--
Formated Sludge + 10.7% $NaNO_3$	80-153	0.01	108+	-10
	153-560	0.24	291-	-144
	560-735	0.03	699+	+45
	735-940	0.03	None	+4
Formated Sludge + Frit	80-210	0.00	154+	+33
	210-560	0.03	296-	-85
	560-713	0.08	None	-1
	713-920	0.01	813+	+78
SGM6	80-153	0.00	124+	+17
	153-560	0.14	326-	-144
	560-713	0.02	638+	+37
	713-940	0.01	792+	+53
SF7	50-190	0.04	125+	+10
	190-645	0.25	293-	-294
	665-755	0.00	None	+20
	787-864	0.00	822, 858-	-33
SF8	50-180	0.03	131+	+10
	180-600	0.28	285-	-266
	617-681	0.02	619, 680-	-44
	>681	0.01	Mulltiple	N.A.
SF9	60-170	0.04	143+	+12
	170-500	0.33	295-	-195
	662-755	0.03	675+	+18
	>755	0.02	Multiple	N.A.

Underlined peaks coincide with TGA differential weight loss peaks.
- indicates exothermic, + indicates endothermic.
N.A. not measureable at high temperatures because of multiple interfering peaks.

TABLE 6:
MAJOR WASTE GLASS REDOX SPECIES AND GLASS MELT RATES

	SAVANNAH RIVER		WEST VALLEY DEMONSTRATION		
SPECIE	**SGM3**	**SGM6**	**SF7**	**SF8**	**SF9**
g mol/ kg glass product					
OXIDIZING SPECIES					
Fe_2O_3	1.23	1.25	1.05	1.08	1.04
MnO	0.38	0.42	0.20	0.19	0.16
$NaNO_3$	0.32	0.78	3.25	3.93	4.00
REDUCING SPECIES					
$C_{12}H_{22}O_{11}$	0	0	0.44	0.59	0.51
HCOOH	1.41	1.13	0	1.04	0.96
MELT RATE					
kg m^{-2} h^{-1} (lb ft^{-2} h^{-1})					
AVERAGE	28* (5.9)*	35* (7.2)*	20 (4.2)	30 (6.2)	33 (6.7)
MAXIMUM	33* (6.8)*	45* (9.3)*	24 (5.0)	38 (7.9)	41 (8.5)

* WITH LID BOOSTER-HEATERS OPERATING

TABLE 7:
FRACTIONAL MASS LOSS AND GAS-TO-GLASS VOLUME RATIO OF A SIMULATED NUCLEAR WASTE GLASS BATCH [32]

TEMPERATURES RANGE, °C	FRACTIONAL MASS LOSS x 10^3	GAS/GLASS VOLUME RATIO
500-700	10	17
700-900	3	6
900-1100	4	10

TABLE 8:
FRACTIONAL MASS LOSS OF CALCINED SIMULATED NUCLEAR WASTE [33]

TEMPERATURE RANGE, °C	FRACTION MASS LOSS x 10^3				
	H_2O	CO_2	NO	O_2	TOTAL (MEASURED)
	(CALCULATED)				
500-700	2	33	1	2	36
700-900	0	0.7	0.03	3	11
900-1000	0	0	0	0.7	1

TABLE 9:

CRITICAL MELTING RATES, N_C, VERSUS FOAM DENSITY AND VISCOSITY

η, Pa s	1	10	100	1000
T, °C	1135	957	818	706
ρ_F, g cm^{-3}	N_C, kg m^{-2} h^{-1}			
0.2	24	18	12	6
0.4	48	36	23	12
0.6	72	54	36	18
0.8	95	72	47	23
1.0	119	89	59	28
N_C from (8):	7900	790	79	8

FIGURE CAPTIONS

Figure 1:
Historical Summary of Glass Melting Technology

Figure 2:
Production Melter Installed at the Savannah River Site, Aiken SC. This is the reference design for the Hanford Waste Vitrification Plant to be built in Hanford WA. Remote maintenance and replacement places size and mass constraints on the system. The waste canister shown is 0.6 m diameter.

Figure 3:
Melt reaction stages for isothermally treated samples from two Savannah River and two West Valley melter tests. See Table 1 for compositions and Table 3 for a description of the stages. The same arrangement of heat treatment time and temperature is used in figures 4 and 5, except the temperature scales are reversed for clarity.

Figure 4:
Effect of batch reaction time and temperature on waste-glass oxygen fugacity and crystallinity.

Figure 5:
Effect of batch reaction time and temperature on durability.

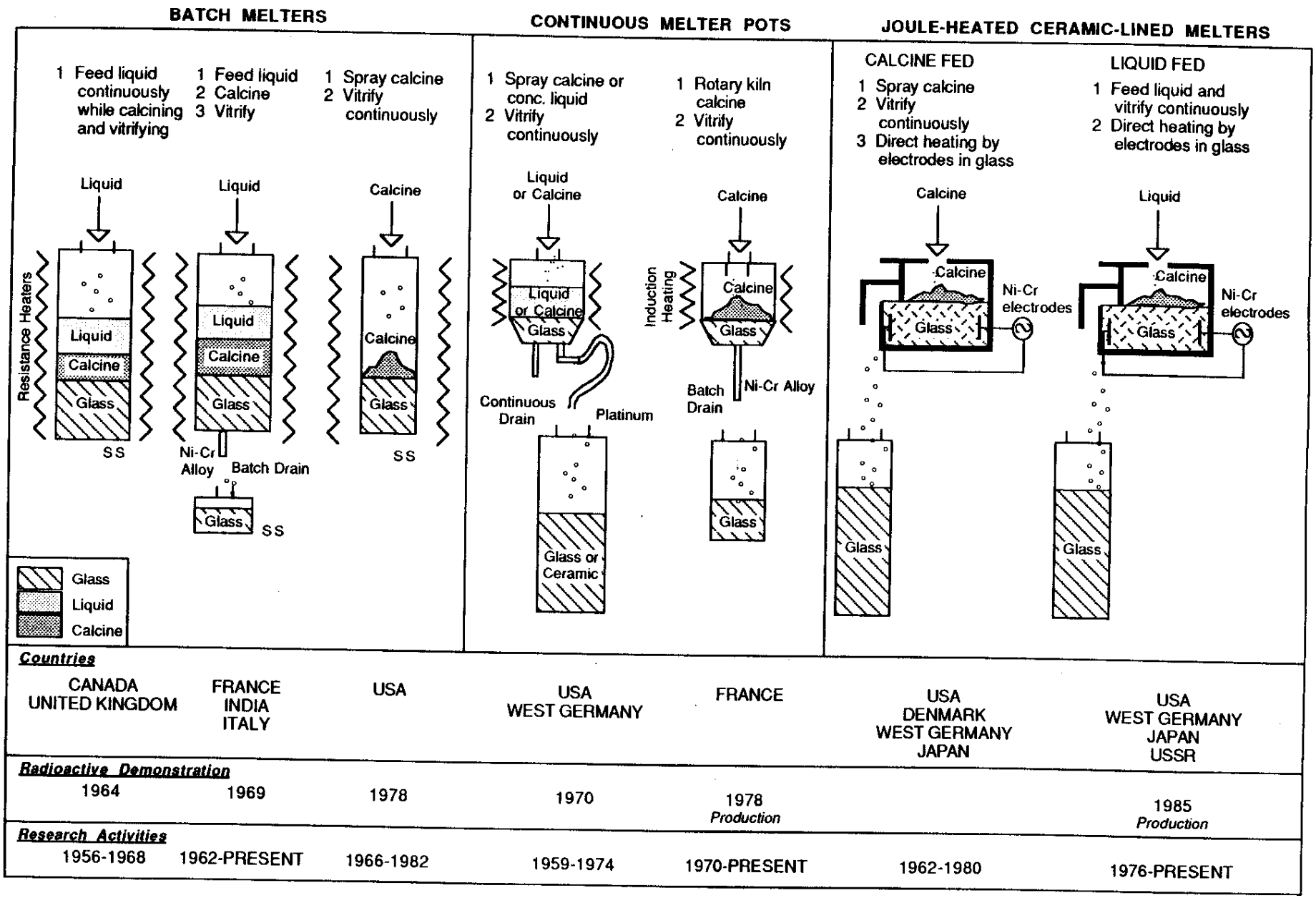

FIGURE 1. Historical Summary of Glass Melting Technology

M90mar051.01

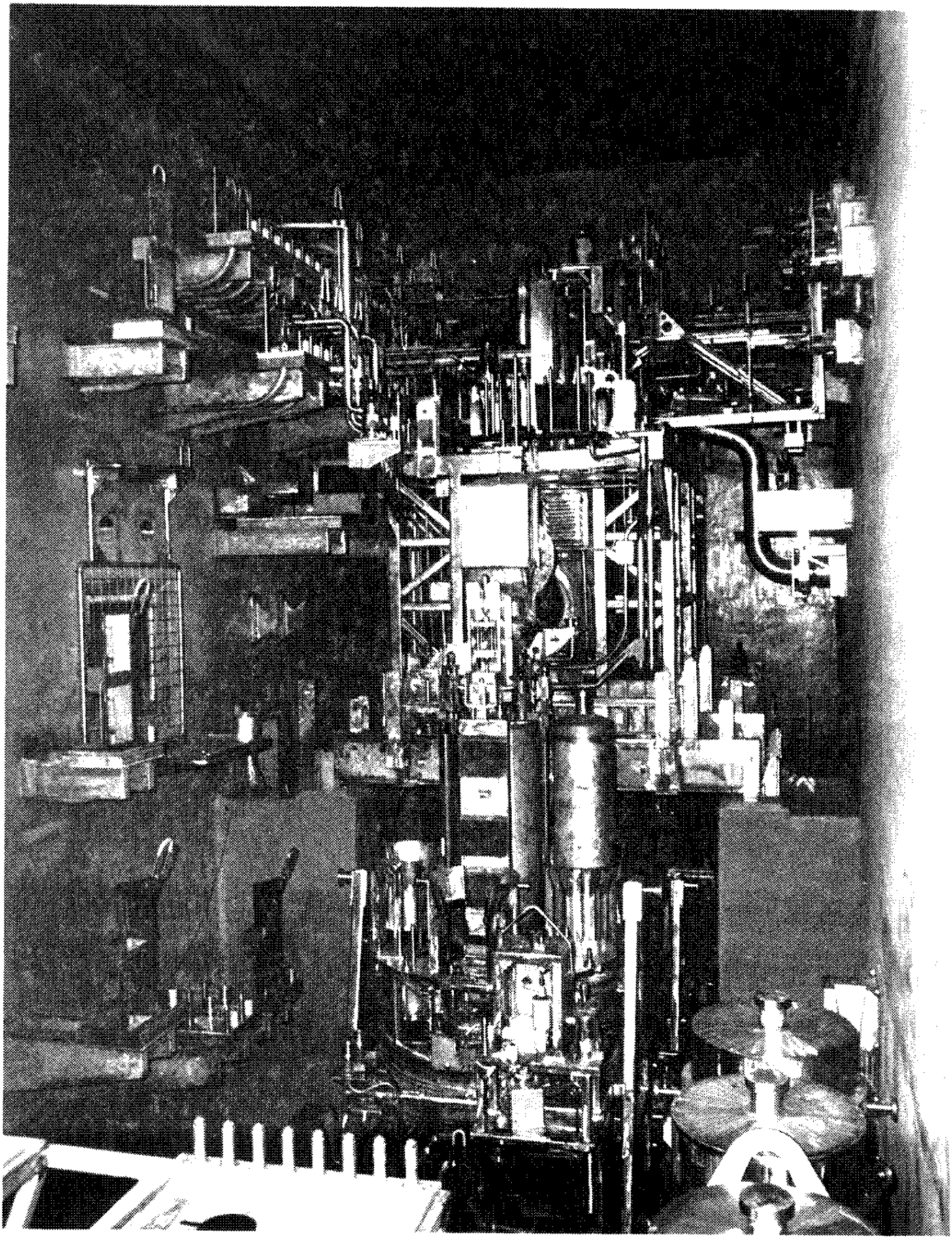

Figure 2:
Production Melter Installed at the Savannah River Site, Aiken SC. This is the reference design for the Hanford Waste Vitrification Plant to be built in Hanford WA. Remote maintenance and replacement places size and mass constraints on the system. The waste canister shown is 0.6 m diameter.

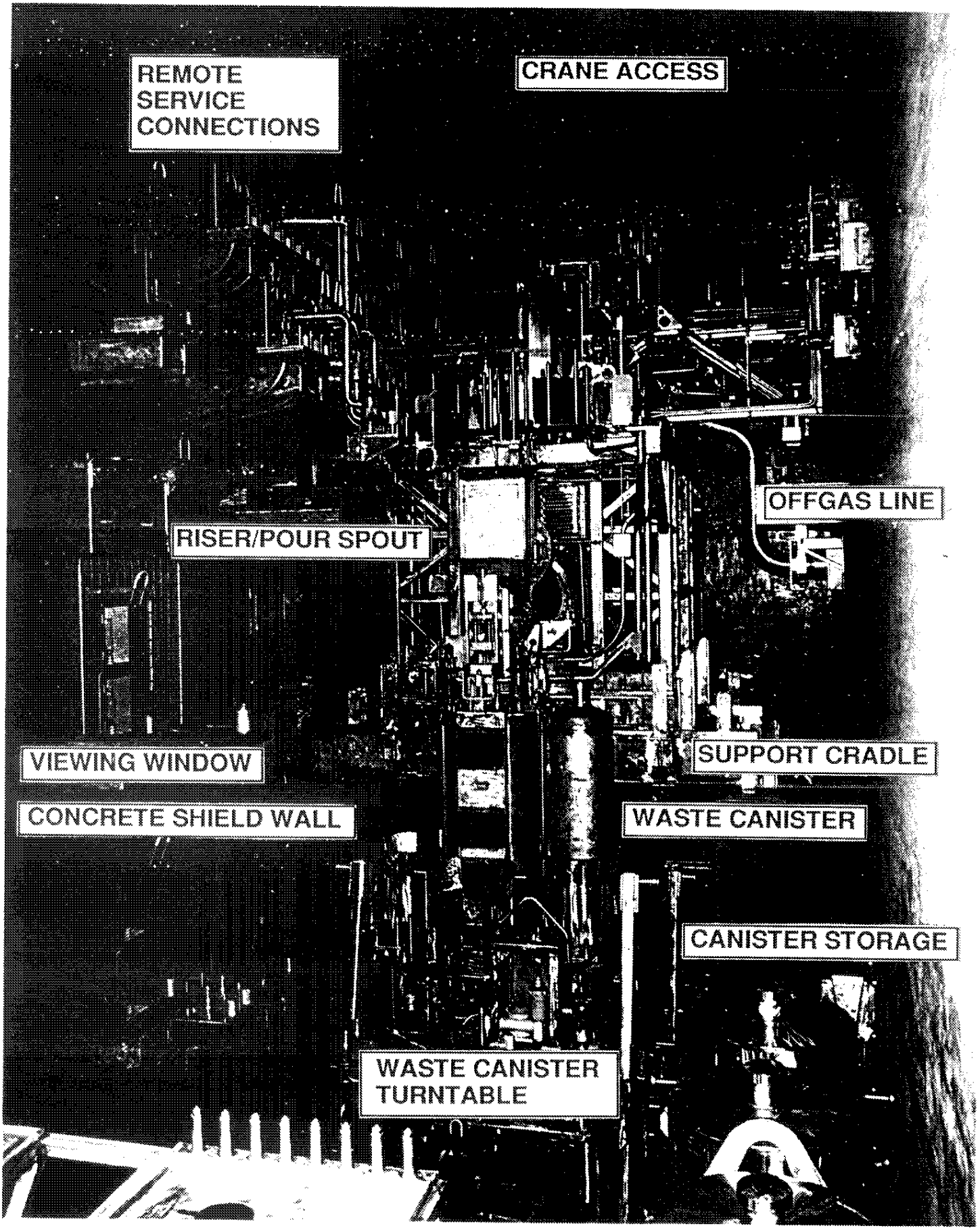
REMOTE SERVICE CONNECTIONS
CRANE ACCESS
OFFGAS LINE
RISER/POUR SPOUT
VIEWING WINDOW
SUPPORT CRADLE
CONCRETE SHIELD WALL
WASTE CANISTER
CANISTER STORAGE
WASTE CANISTER TURNTABLE

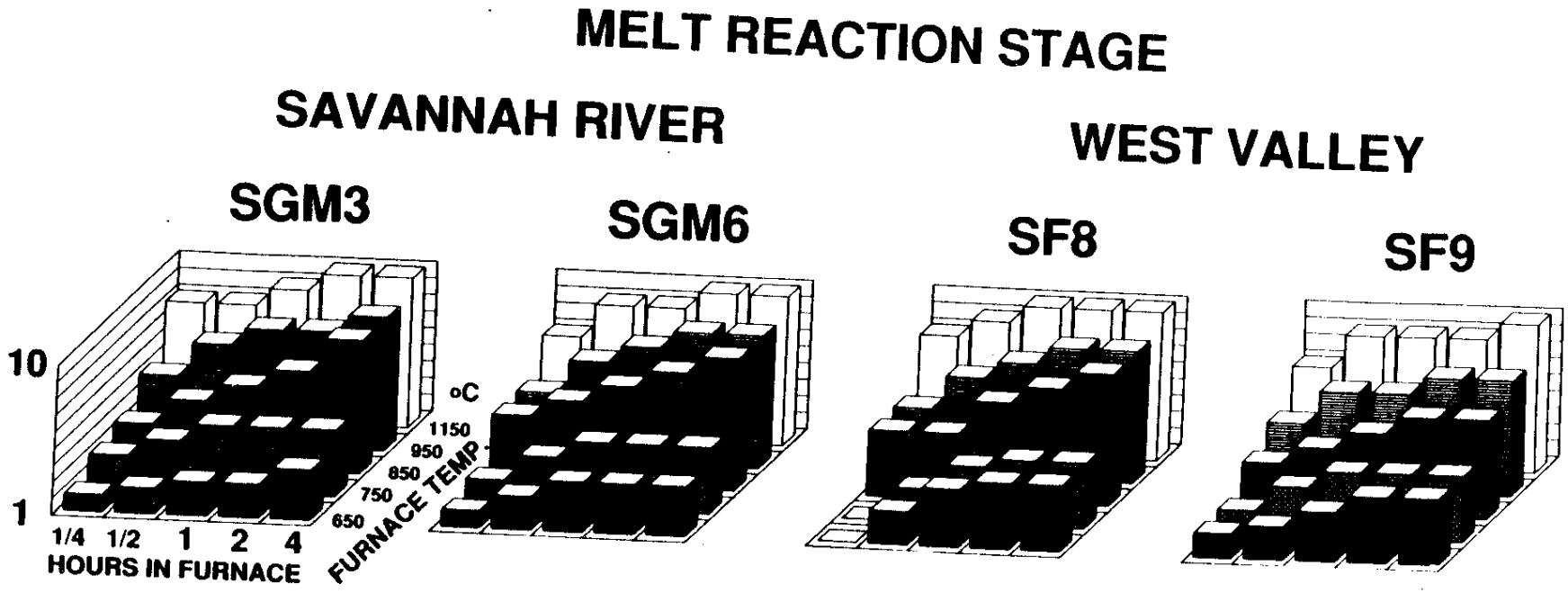

Figure 3:
Melt reaction stages for isothermally treated samples from two Savannah River and two West Valley melter tests. See Table 1 for compositions and Table 3 for a description of the stages. The same arrangement of heat treatment time and temperature is used in figures 4 and 5, except the temperature scales are reversed for clarity.

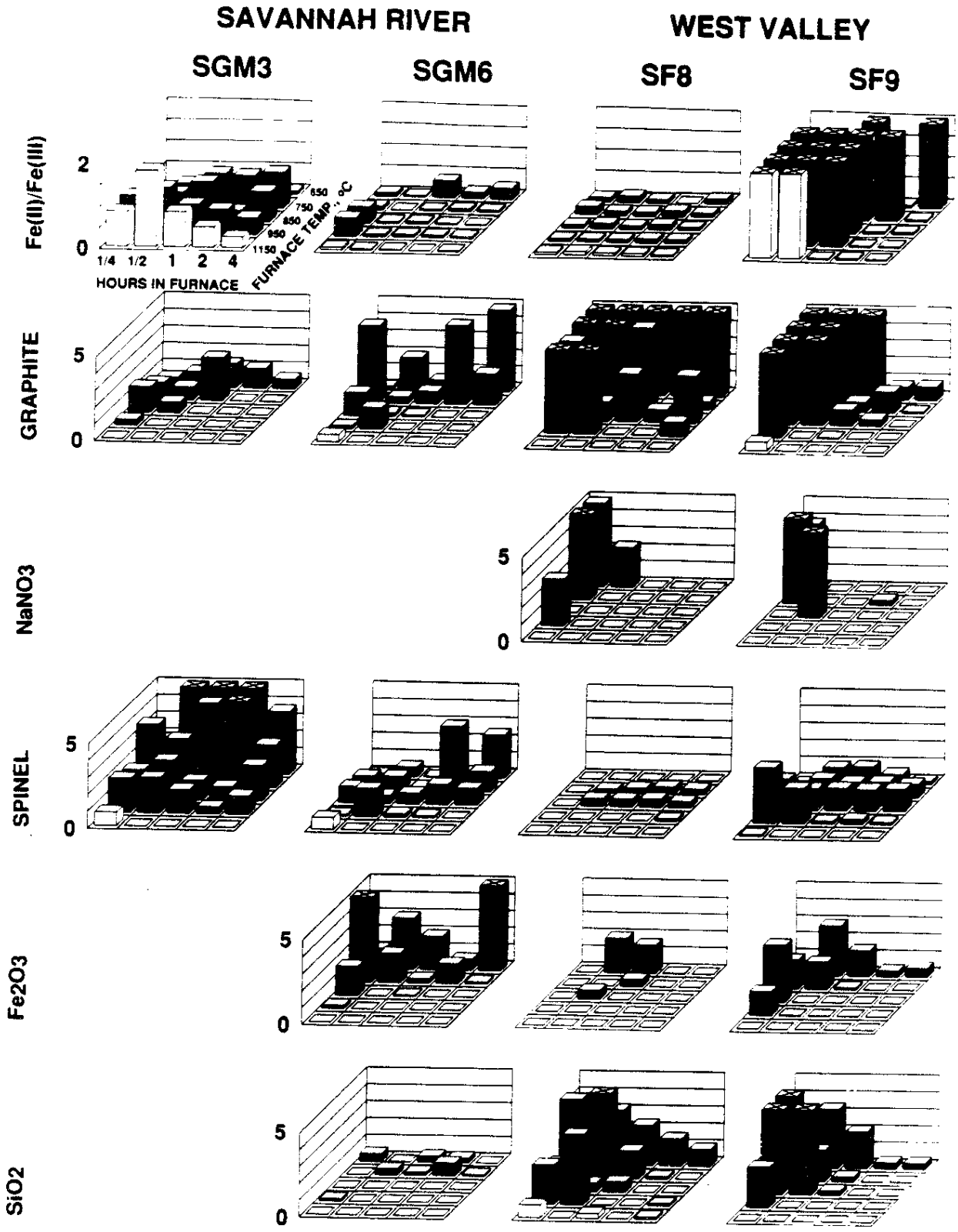

Figure 4:
Effect of batch reaction time and temperature on waste-glass oxygen fugacity and crystallinity.

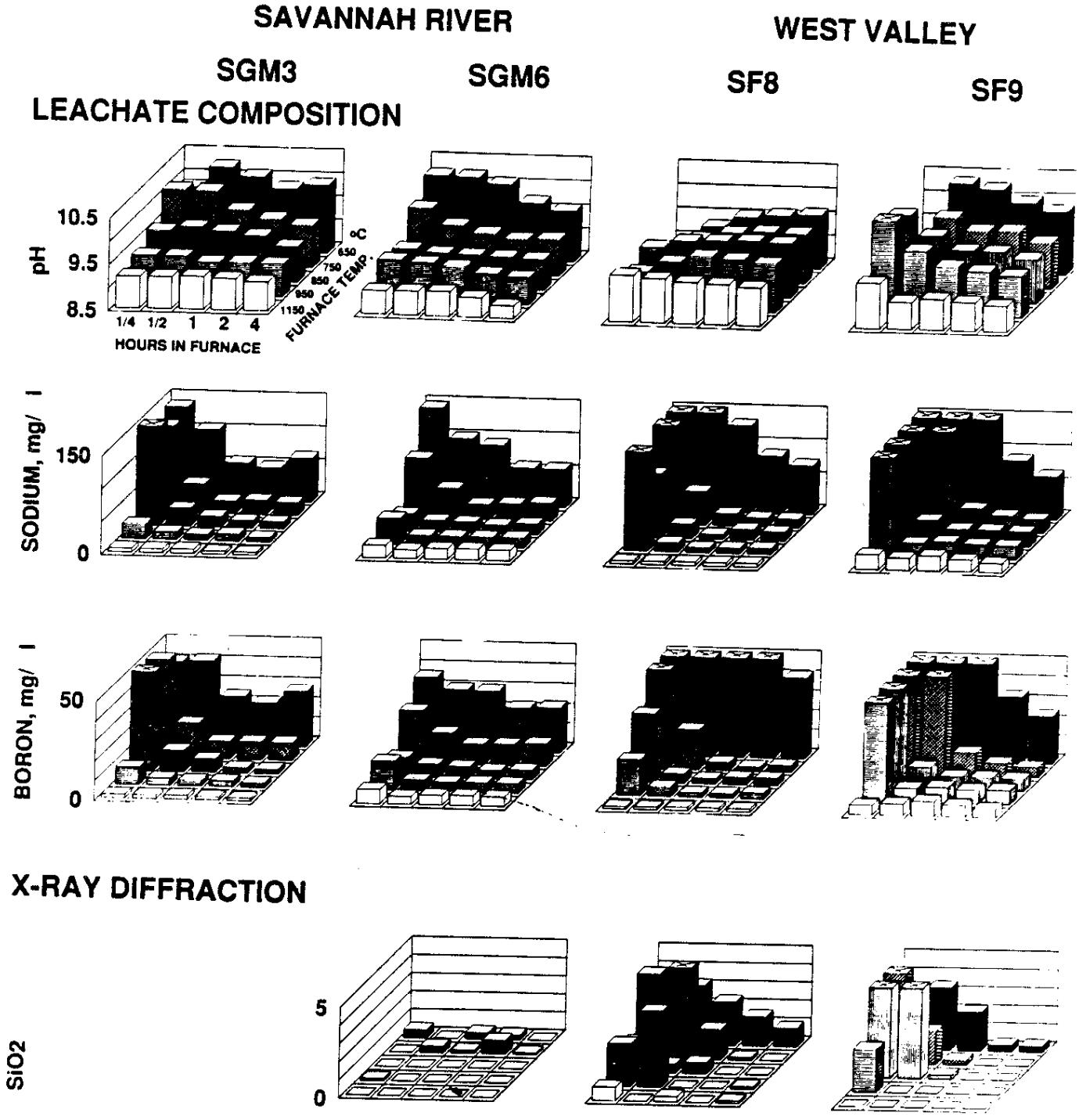

Figure 5:
Effect of batch reaction time and temperature on durability.